

Title no. 98-S50

Static Behavior of Anchors under Combinations of Tension and Shear Loading

by Dieter Lotze, Richard E. Klingner, and Herman L. Graves, III

A research project has recently been completed that had the objective of determining how the seismic behavior and strength of anchors (cast-in-place, expansion, and undercut) and their supporting concrete differ from the static behavior. To that end, a research program was carried out on the dynamic behavior of anchors (fasteners) to concrete. The research program comprised four tasks: 1) static and dynamic behavior of single tensile anchors (250 tests); 2) static and dynamic behavior of multiple tensile anchors (179 tests); 3) static and dynamic behavior of near-edge anchors (150 tests); and 4) static and dynamic behavior of multiple-anchor connections (16 tests). The anchors tested were selected based on their reported frequency of use in nuclear power plants in the U.S. Anchors included cast-in-place headed bolts, grouted headed bolts, two wedge-type expansion anchors, one sleeve-type expansion anchor, and two undercut anchors. Loading conditions included tension, shear, and combined tension and shear. Test variables included different concrete strengths and types, loading rate, and the presence of cracks. This paper deals with the static behavior of single and multiple undercut and sleeve anchors placed in uncracked concrete and loaded by combinations of tension and shear. The results are used to draw conclusions regarding force and displacement interaction diagrams for single anchors and the applicability of elastic and plastic theory to the design of multiple-anchor connections to concrete.

Keywords: anchor; anchor bolt; dynamic loading; embedment length; static load.

OBJECTIVES AND SCOPE

A research program has recently been completed that had the objective of obtaining technical information to determine how the seismic behavior and strength of anchors (cast-in-place, expansion, and undercut) and their supporting concrete differ from the static behavior. The research program comprised four tasks:

1. Static and dynamic behavior of single tensile anchors (250 tests);
2. Static and dynamic behavior of multiple tensile anchors (179 tests);
3. Static and dynamic behavior of near-edge anchors (150 tests); and
4. Static and dynamic behavior of multiple-anchor connections (16 tests).

This paper deals with part of Task 2, which concerns the static behavior of single and multiple undercut and sleeve anchors placed in uncracked concrete and loaded by combinations of tension and shear. The results are used to draw conclusions regarding force and displacement interaction diagrams for single anchors and regarding the applicability of elastic and plastic theory to the design of multiple-anchor connections to concrete.

The anchors tested were selected based on their reported frequency of use in nuclear power plants in the U.S. Anchors

included cast-in-place headed bolts, grouted headed bolts, two wedge-type expansion anchors, one sleeve-type expansion anchor, and two undercut anchors. Loading conditions included tension, shear, and combined tension and shear. Test variables included different concrete strengths and types, loading rate, reinforcement, and the presence of cracks.

BACKGROUND

In CEB (1991), research on fastening technology is extensively described. Further summaries are included in Eligehausen et al. (1989) and Rehm, Eligehausen, and Mallée (1992). Of those results, only those essential for the present research are reviewed briefly as follows. Emphasis is placed on the influence of loading direction and loading rate on the ultimate capacity and the load-deformation behavior of single anchors failing by concrete breakout or by fracture of the anchor shank.

Failure mode and displacement under tension and shear

Anchor bolts or headed studs can fail in the anchor itself or in the concrete. Most steel failures are failure of the anchor shank, failure of the anchor sleeve, or both. Possible modes of concrete failure are concrete breakout, splitting of the base concrete to the loading direction for near-edge anchor groups, or pullout of the anchors due to local failure of the concrete. The latter depends on the available bearing area and also on the concrete strength of undercut anchors and headed studs. Pullout can also occur with torque-controlled expansion anchors, depending on the geometry and the coefficient of friction in the expansion zone. In pull-through failure, the cone is pulled through the sleeve of the anchor. Finally, a shallow anchor can fail in shear by formation of a shallow concrete breakout cone on the side of the anchor opposite to the direction of the applied load. Under shear loading, an additional possibility is local, shell-shaped concrete spalling in front of the anchor.

The displacement of anchors depends on the deformation of the attachment, of the anchors, and of the concrete in which the anchors are embedded. Prior analytical investigation of the deformation of anchors addressed only a few anchor types, loaded in concentric tension. The work of Fuchs (1990) provides some useful information regarding shear behavior.

ACI Structural Journal, V. 98, No. 4, July-August 2001.

MS No. 00-177 received August 17, 2000 and reviewed under Institute publication policies. Copyright © 2001, American Concrete Institute. All rights reserved, including the making of copies unless permission is obtained from the copyright proprietors. Pertinent discussion will be published in the May-June 2002 *ACI Structural Journal* if received by January 1, 2002.

Dieter Lotze is Director of Research for Halfen GmbH & Co., Wiemsheim, Germany, and is a former visiting scholar at the University of Texas at Austin, Tex.

Richard E. Klingner, F.A.C.I., is the Phil M. Ferguson Professor in Civil Engineering at the University of Texas at Austin. He is a former chair ACI Committee 531, Masonry Structures Research, and Joint ACI-ASCE Committee 442, Response of Concrete Buildings to Lateral Forces. He is a member of ACI Committees 349, Concrete Nuclear Structures; 355, Anchorage to Concrete; 374, Performance-Based Seismic Design of Concrete Buildings; 523, Cellular Concrete; and Joint ACI-ASCE-TMS Committee 530, Masonry Standards. He is also a former member of ACI's Technical Activities Committee (TAC), and a current member of ACI's Educational Activities Committee (EAC). His research interests include dynamic response of masonry and concrete structures, and anchorage to concrete.

Herman L. Graves, III is a senior engineer at the Office of Nuclear Regulatory Research, U.S. Nuclear Regulatory Commission, Washington, D.C.

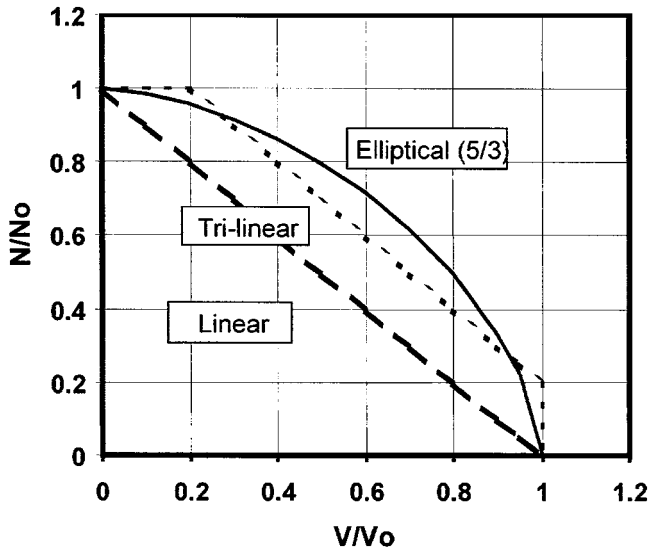


Fig. 1—Tension-shear force interaction for anchors.

Ultimate capacity under tension or shear

As discussed in Fuchs, Eligehausen, and Breen (1995), mean concrete breakout capacity in tension in uncracked concrete is well-predicted by Eq. (1)

$$N_n = k \sqrt{f_c} h_{ef}^{1.5} \quad (1)$$

where

N_n = mean tensile capacity, N;
 k = 15.0 for expansion anchors, 17.0 for headed anchors;
 f_c = cylinder compressive strength of concrete, MPa; and
 h_{ef} = effective embedment depth, mm.

Equation (1) is valid for single anchors with an edge distance of at least $1.5h_{ef}$. A member thickness of at least $2h_{ef}$ is assumed. In cracked concrete, ultimate capacity decreases by approximately 30%.

As discussed in Fuchs, Eligehausen, and Breen (1995), mean concrete breakout capacity in shear in uncracked concrete is well-predicted by Eq. (2)

$$V_n = 1.0 \left(\frac{d_o}{\ell} \right)^{0.2} \sqrt{f_c} c_1^{1.5} \quad (2)$$

where

d_o = anchor diameter (including sleeve if present), mm;
 ℓ = embedment length, mm; and

c_1 = edge distance in the loading direction, mm.

In Eq. (2), a member thickness of at least $1.4c_1$ is assumed. Group and edge effects are addressed by the CC method (Fuchs, Eligehausen, and Breen 1995).

Tensile capacity as governed by steel failure is given by the product of the ultimate tensile strength and the cross-sectional area of the anchor shank

$$N_n = A_s f_{ut} \quad (3)$$

For a uniform cross section, the ratio of shear to tensile capacity is (Cook and Klingner 1992)

$$\left(\frac{V_n}{N_n} \right) \approx 0.6 \quad (4)$$

If the anchor sleeve goes through the baseplate, steel capacity in shear is increased by an amount that depends on the degree of interaction between the anchor shank and sleeve and on the material of each component. Current technical literature does not address this.

Tension-shear force interaction

Figure 1 shows different models for the interaction of tension and shear capacities.

For failure by steel fracture, an elliptical interaction is used

$$\left(\frac{N}{N_0} \right)^p + \left(\frac{V}{V_0} \right)^p = 1 \quad (5)$$

The exponent p varies between 5/3 (McMackin, Slutter, and Fishere 1973) and 2.0 (Shaikh and Whayong 1985). For failure by concrete breakout, Johnson and Lew (1990) propose a linear interaction as a lower bound (Fig. 1). Bode and Roik (1987) propose a tri-linear interaction (Eq. (6a) through (6c))

$$\left(\frac{N}{N_0} \right) = 1 \quad (6a)$$

$$\left(\frac{V}{V_0} \right) = 1 \quad (6b)$$

$$\left(\frac{N}{N_0} \right) + \left(\frac{V}{V_0} \right) = 1 \quad (6c)$$

The elliptical interaction of Eq. (5) has been proposed for concrete failure as well, using an exponent p equal to 4/3 (PCI 1985), 5/3 (Cook and Klingner 1992), or 2.0 (Shaikh and Whayong 1985).

Where failure modes in tension and shear differ, the previously mentioned interaction relations are probably conservative. It is possible that behavior could be better described by using separate interaction relations for each individual failure mode and by determining the critical oblique capacity separately for each failure mode. The smaller of the values for each failure load would then determine the governing failure mode and the corresponding capacity. Further study of this subject is one objective of the work described herein.

Tension-shear displacement interaction

Displacement interaction has not been widely investigated and is not required for the elastic design procedure in which no redistribution of anchor forces is assumed. Elastic design of critical cases (such as a row of anchors placed perpendicular to the edge of a structural member and loaded in shear) can be addressed by special provisions. If redistribution of anchor forces is assumed, as in the plastic design approach, then knowledge of displacement interaction is necessary.

Dieterle et al. (1989) report test results for different types of anchors in 0.4 mm cracks subjected to loads in different directions and to different independent histories of tension and shear displacement. The embedment length and edge distance were chosen so that, for loading angles exceeding 30 degrees from the anchor axis, the failure mode shifted from concrete breakout (under pure tension) to steel failure (in pure shear). Thus, a complete set of load-displacement curves did not exist with the same failure mode over the entire range of loading angles. In those tests, concrete compressive strengths varied between 27 and 33 MPa. Figure 2 shows the interaction of displacements for undercut anchors (Dieterle et al. 1989). The figure refers to anchors with flush-sleeve installation (sleeve flush with the surface of the concrete), failing by concrete breakout under pure tension and by steel fracture under pure shear.

Figure 2 shows a distinct maximum of the combined displacement at failure at a loading angle of about 30 to 45 degrees. Anchors loaded at that angle exhibit steel fracture but withstand more displacement than anchors loaded in pure shear. Generally, the failure displacement is greater in shear than in tension. This is because shell-shaped concrete spalling occurs in front of the anchor in the loading direction, permitting increased shearing deformation.

Capacity of multiple-anchor connections to concrete

The capacity of multiple-anchor connections to concrete, loaded by combinations of moment and shear, depends on the capacities of the individual anchors in combined tension and shear and also on the assumed distribution of actions from the attachment to the anchors. A variety of approaches are available for calculating this distribution. In principle, these lie between two limiting approaches:

1. One limit is the elastic approach, in which loads are assumed to be distributed to the anchors in proportion to their stiffness. A connection capacity predicted using the elastic approach is in theory conservative; by the lower-bound theorem of structural analysis, it satisfies equilibrium and stress-strain relationships and nowhere exceeds the anchor strength. The elastic approach neglects the effects of inelastic redistribution of anchor actions; and

2. The other limit is the plastic approach, in which loads are assumed to be distributed to the anchors in proportion to their strengths. A connection capacity predicted using the plastic approach may be unconservative; by the upper-bound theorem of structural analysis, it satisfies equilibrium and anchor strengths but not necessarily stress-strain relationships. The plastic approach neglects any possible limitation on the inelastic redistribution of anchor actions.

Current design provisions for multiple-anchor connections to concrete (IBC 2000) prescribe the elastic approach as a default, and also permit the plastic approach provided that the deformation capacity of the anchors is checked. Details of the elastic and plastic approaches are presented in Fuchs,

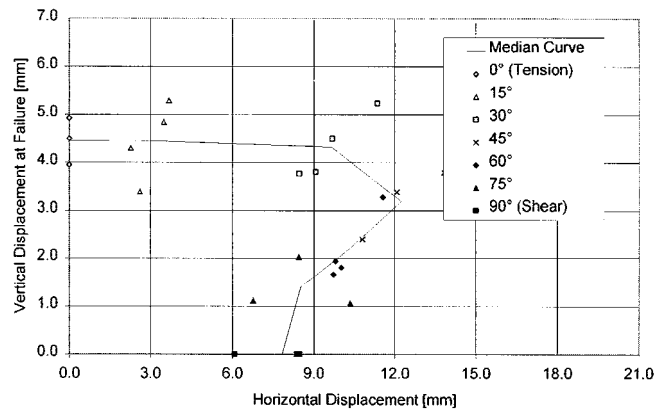


Fig. 2—Tension-shear displacement interaction of undercut anchor (Dieterle 1989).

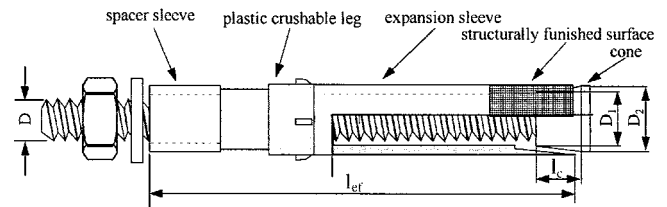


Fig. 3—Key dimensions of sleeve anchor.

Eligehausen, and Breen (1995) and Cook and Klingner (1992), respectively. Later in this paper, test results for multiple-anchor connections to concrete are compared with the predictions of each limiting approach.

TEST SETUPS AND PROCEDURES

Anchors tested

Based on surveys of existing anchors in nuclear applications, the NRC was primarily interested in documenting the behavior of selected wedge-type expansion anchors, of selected undercut anchors, and also of anchors in cementitious grout. The tests described here involved one undercut anchor (Undercut Anchor 1 [UC1]) and a heavy-duty, sleeve-type, single-cone expansion anchor (sleeve anchor). Based on current use in nuclear applications, it was decided to test anchors ranging in diameter from 3/8 to 1 in. (9.2 to 25.4 mm), with emphasis on the 3/4 in. (19.1 mm) diameter.

Sleeve anchor—The sleeve anchor tested throughout this study is a single-cone, sleeve-type expansion anchor with follow-up expansion capability, as shown in Fig. 3. The configuration of this anchor is more complex than that of wedge-type expansion anchors. The anchor is set in a predrilled hole and torqued to raise the cone and expand the sleeve. Sleeve anchors with 20 mm diameter have a step inside the expansion sleeve. Sleeve anchors with 10 mm diameter have no such step. Key dimensions of the sleeve anchor are shown in Table 1.

Undercut Anchor 1—The UC1s tested throughout this study is a conventionally opening undercut anchor, consisting of a threaded rod with a steel cone at one end and an expansion sleeve. Key dimensions of UC1 are shown in Fig. 4 and Table 2. Using a universal testing machine, Lotze and Klingner (1997) performed three tension tests in Task 2 of this program (as listed in the Objectives and Scope section of this paper) on three shafts of a 5/8 in. (16 mm) UC1. The average ultimate strength was 912 MPa (132 kips). The actual bearing area of UC1 anchors (the surface area of the under-

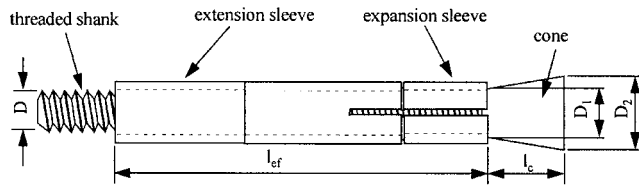


Fig. 4—Key dimensions of UC1.

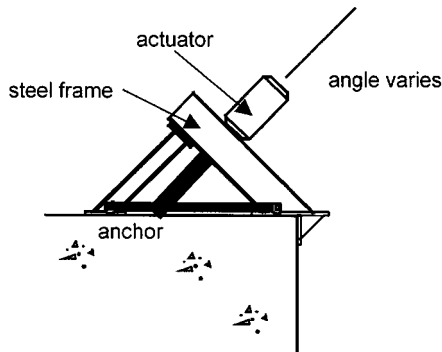


Fig. 5—Test setup for anchors loaded at different orientations.

Table 1—Key dimensions of sleeve anchor

Anchor diameter D		Sleeve diameter		l_{ef}		D_1		D_2		l_c	
in.	mm	in.	mm	in.	mm	in.	mm	in.	mm	in.	mm
3/8	10	0.563	14.3	2.25	57.2	0.48	12.2	0.58	14.7	0.43	10.9
3/4	20	1.070	27.3	4.00	102.0	0.92	23.4	1.09	27.7	0.55	14.0

Table 2—Key dimensions of UC1

Anchor diameter D		Sleeve diameter		l_{ef}		D_1		D_2		l_c	
in.	mm	in.	mm	in.	mm	in.	mm	in.	mm	in.	mm
3/8	10	0.625	15.9	2.25	57.2	0.440	11.2	0.625	15.9	0.600	15.2
5/8	16	0.910	23.1	7.00	178.0	0.720	18.3	0.940	23.9	0.800	20.3
3/4	19	1.105	28.1	4.00	102.0	0.815	20.7	1.140	29.0	0.915	23.2

cut portion of the sleeve) is 3.25 in.² (2097 mm²) for 3/4 in. (19 mm) diameter anchors, 1.79 in.² (1153 mm²) for 5/8 in. (16 mm) diameter anchors, and 1.23 in.² (794 mm²) for 3/8 in. (10 mm) diameter anchors.

Embedment depths

The objective of this part of Task 2 was to examine the effect of different combinations of tension and shear loading on the behavior of anchors, as governed by steel failure and combinations of steel and concrete breakout failure. Therefore, some anchors had relatively deep embedments, while others had more shallow ones. The embedment depths used are described when each set of test results is discussed.

Concrete

The target concrete compressive strength for this testing program was 4700 lb/in.² (32.4 MPa), with a permissible tolerance of ± 500 lb/in.² (± 3.45 MPa) at the time of testing. This target value was selected because it is representative of concrete strengths in existing nuclear power plants. Mixture proportions are shown in Table 3. For the tests described here, a porous limestone aggregate was used.

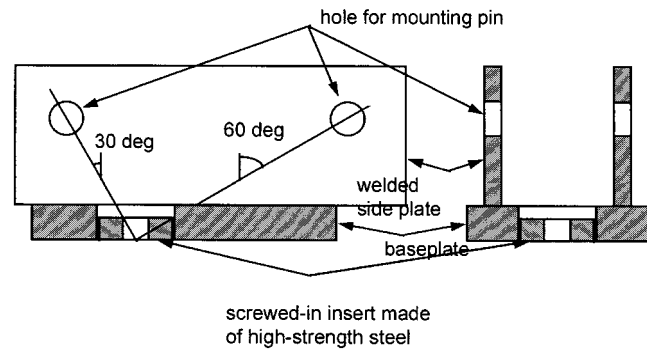


Fig. 6—Special loading shoe for tests at different orientations.

Table 3—Concrete mixture proportions

Concrete	Concrete mixture proportions				
	Cement, lb/yd ³	Coarse aggregate, lb/yd ³	Fine aggregate, lb/yd ³	Water, lb/yd ³	Retarder, oz/yd ³
3000 lb/in. ² limestone	360	1884	1435	266	10.5
4700 lb/in. ² limestone	390	1876	1432	250	48.0

The mixture was proportioned to have a 6 in. (152 mm) slump. In the Task 1 tests of this program, however, it was found that concrete mixture with a 6 in. slump often had lower strength than 4200 lb/in.² (29.0 MPa) at 28 days. For that reason, later specimens were cast with a 4 in. (101 mm) slump.

The limestone aggregate used is very porous. Depending on its moisture content, the water-cement ratio in the concrete mixture can vary widely. To control the water content, the limestone aggregate had to be sprinkled several days before casting.

All test specimens were cast using ready-mix concrete, consolidated with mechanical vibrators, screeded, troweled, and covered with polyethylene sheets. Eighteen 6 in. (152 mm) diameter by 12 in. (305 mm) cylinders were usually cast with the test specimens and cured in laboratory air. The specimens were not tested until at least 28 days after casting and until the desired strength had been reached.

Test setup for Task 2 (single anchors loaded at different orientations)

The typical test specimen was a concrete block 39.5 in. (1 m) wide, 24 in. (0.6 m) deep, and 87.5 in. (2.2 m) long. Seven No. 6 (32 mm) longitudinal reinforcing bars were placed in the middle of each block to provide safety when the block was moved. This reinforcement was placed at the midheight of the block to permit testing anchors on both the top and bottom surfaces while precluding interference with anchor behavior. Four lifting loops were located at the midheight of the blocks, permitting transport by overhead crane.

The test setup consisted of a structural steel framework holding a center-hole actuator at a variable angle (Fig. 5). Load was applied through a special loading shoe, shown in Fig. 6.

Static tensile loads were applied by a hand pump connected to a 60 ton (534 kN) center-hole hydraulic ram. Applied load was measured by a load cell placed against the ram. Anchor displacements parallel and perpendicular to the surface of the block were measured by linear potentiometers attached

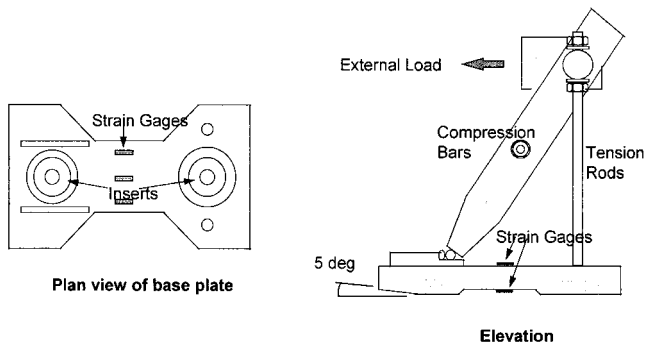


Fig. 7—Loading fixture for eccentric shear tests on two-anchor attachments.

to the surface of the block, and resting against thin glass plates attached to the loading shoe.

Test setup for Task 2 (eccentric shear tests on two-anchor attachments)

The loading fixture consisted of a special baseplate with two high-strength steel inserts, two tension rods, and two compression bars (Fig. 7). The inside thickness of these inserts was counter-bored to 3/4 in. (19 mm), the same as the diameter of the anchor bolts. The diameter of the baseplate holes was 13/16 in. (20.6 mm). The overall test setup is shown in Fig. 8.

The tension rods and compression bars were connected at the top by a threaded portion of the loading rod to transmit the external shear load. The center section of the baseplate was machined narrower and thinner than the rest of the plate to achieve uniform stress distribution and to avoid direct contact with the concrete surface. The other ends of the compression bars rested on a circular steel bar, located so that the extension of the centerline of the compression bars would pass through the point of contact between the front insert and the anchor shank. As shown in Fig. 7, the compression end of the loading plate was beveled at 5 degrees from the front edge of the front hole to eliminate prying action on the compression anchors during testing, and also to reduce the bending moment in the baseplate caused by the force in the compression bars. The tension rods were placed at the same distance from the compression edge as the tension anchor to eliminate any moment caused by the forces in them.

The axial force and bending moment in the baseplate were calculated from strain measurements from two sets of three strain gauges each, evenly spaced on the top and bottom of the center section of the baseplate. The width of the baseplate was reduced to 4 in. (101.6 mm) in this region to achieve a more uniform stress distribution. Due to limited data acquisition capacity, only the outside two pairs were used.

Using this loading apparatus, horizontal load is transferred through the compression bars to the front end of the baseplate. The force measured by the strain gages equals the shear force acting on the back anchor. As a result, the shear distribution between the two anchors can be determined experimentally, and the computed tension force on the back anchor can also be modified using the moment at the center of the baseplate.

Based on the geometry of the loading apparatus, the force in the tension rods is 1.2 times the external shear load. Therefore, as shown in Fig. 9, the tension force on the back anchor

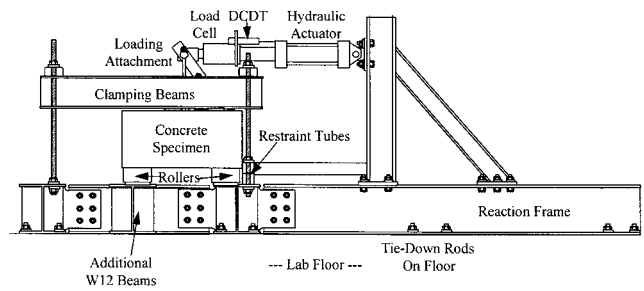


Fig. 8—Setup for eccentric shear tests on two-anchor attachments.

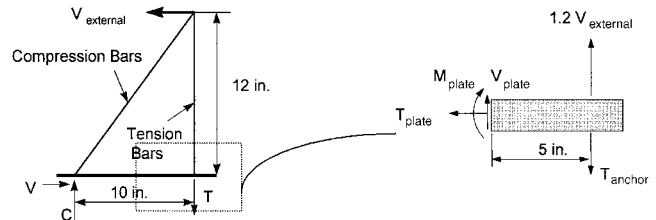


Fig. 9—Free-body diagram of loading apparatus for eccentric shear tests on two-anchor attachments.

can be calculated by equilibrium of moments about the center of the baseplate.

$$(1.2 \cdot V_{\text{external}} - T_{\text{anchor}}) \cdot (5 \text{ in.}) + V(0) = M_{\text{plate}} \quad (7)$$

$$T_{\text{anchor}} = 1.2 \cdot V_{\text{external}} - M_{\text{plate}}/5 \text{ in.} \quad (8)$$

The shear force on the back anchor equals the measured tension force in the baseplate T_{plate} . The external load on the connection was measured with a load cell using a spherical bearing to eliminate error due to angular deviation. The tension forces on each anchor were measured with force washers placed between the normal washers and the baseplate.

The displacements of the baseplate were described in terms of horizontal slip and rotation. Baseplate slip was measured with a potentiometer placed against the back of the baseplate. The horizontal displacement of the loaded point 12 in. (305 mm) from the surface was also measured. The vertical displacement of the baseplate δ_v was measured at the centerline of the baseplate. This, however, may not be exact, due to the uneven concrete surface and the flexibility of the baseplate. The rotation of the attachment was calculated from the difference between the transverse displacements measured at the level of the baseplate and at 12 in. (305 mm) above the concrete surface. This procedure in effect assumes the attachment to be infinitely stiff. The rotation was also calculated using the vertical displacement measured at the center of the baseplate. The results of these two calculations were almost identical.

Data from the load cell and the displacement transducers were fed to a multichannel scanner, downloaded to a microcomputer, and reduced using conventional spreadsheet programs.

Test procedure

1. Position baseplate so anchors contact sides of the anchor hole away from the load; torque anchors;

Table 4—Average loads and displacements at failure for Series 2.3

Test	Anchor	Loading angle, degrees	Concrete strength, MPa	Failure load, kN	Horizontal displacement, mm	Vertical displacement, mm	Surface dimension of shell-shaped spalling, mm
23H64*	Sleeve, M16, flush-sleeve installation	Tension	32.4	126.2	0.00	21.20	—
		15	32.4	127.5	7.34	9.67	28
		30	32.4	106.6	4.02	2.08	11
		45	32.4	89.7	4.14	1.26	6
		60	32.4	83.2	3.66	0.85	2
		90	32.4	78.0	3.14	0.09	0
23H74	Sleeve, M16, through-sleeve installation	30	32.4	136.8	19.65	10.96	38
		45	32.4	137.0	27.77	11.56	43
		60	32.4	138.1	15.96	5.22	35
		90	32.4	149.7	15.02	2.35	13
23M54	UC1, 5/8 in. (16 mm), flush-sleeve installation	Tension	32.4	135.3	0.00	21.34	—
		15	32.4	126.6	9.07	10.33	21
		30	32.4	112.2	6.65	3.46	13
		45	32.4	93.5	6.91	2.00	9
		60	32.4	86.2	6.40	1.11	6
		90	32.4	82.2	5.69	0.00	2
23M74	UC1, 5/8 in. (16 mm), through-sleeve installation	30	32.4	145.0	21.11	11.34	51
		45	32.4	133.2	20.09	6.07	35
		60	32.4	131.9	25.85	6.97	38
		90	32.4	155.9	13.65	0.00	8
23M53†	UC1, 5/8 in. (16 mm), flush-sleeve installation	Tension	20.7	134.8	0.00	41.13	—
		15	20.7	130.2	18.61	19.82	35
		30	20.7	106.8	14.86	6.63	25
		45	20.7	95.2	9.61	2.70	18
		60	20.7	84.4	9.42	1.79	14
		90	20.7	80.4	6.18	0.21	5
23M34	UC1, 3/8 in. (9.5 mm), flush-sleeve installation	Tension	32.4	50.6	0.00	1.96	—
		15	32.4	44.6	2.26	1.85	0
		30	32.4	38.7	2.86	1.11	0
		45	32.4	35.2	2.51	0.49	0
		60	32.4	30.8	2.66	0.36	0
		90	32.4	30.0	2.58	0.15	0

*Pull-through failure for three of four anchors; steel fracture bar for one at load 140.1 kN, vertical displacement 20.98 mm.

†Mean value for tests with steel failure only (two out of three).

2. Connect loading plate to horizontal loading rod, install clamping beams, and position gages;

3. Conduct the test; and

4. After connection failure, remove data acquisition equipment. Transfer data to computer and save.

All tests were quasistatic. Load was applied slowly under displacement control, while monitoring the load cell to avoid any sudden increase of the load, until the connection failed.

TEST RESULTS FOR ANCHORS UNDER COMBINATIONS OF TENSION AND SHEAR LOADING

Results for single anchors loaded at different orientations (Series 2.3 and 2.4)

The average loads and displacements at failure for each test are compared in Table 4 for Series 2.3, and in Table 5 for Series 2.4.

In Series 2.3 (Table 4), 5/8 in. (16 mm) anchors had effective embedment depths of 178 mm, and 3/8 in. (9.5 mm) anchors had effective embedment depths of 89 mm. In Table 4, M16 sleeve anchors had an initial torque of 203 Nm, reduced to half that value before testing, while M16 UC1s had an initial torque of 244 Nm, reduced to half that value before

testing. M9.5 UC1s had an initial torque of 54 Nm, reduced to half that value before testing.

In Series 2.4 (Table 5), the anchors were M16 UC1 with flush-sleeve installation, an effective embedment depth of 178 mm, a concrete strength of 32.4 MPa, and an initial torque of 244 Nm, reduced to half that value before testing. In some tests, a torque of only 203 Nm instead of 244 Nm was applied to avoid splitting of the concrete edge.

Detailed results, load-displacement curves and their mathematical description, photos of failure modes, and interaction diagrams for loads and displacements are given in Appendixes 36 to 144 of Lotze and Klingner (1997). The appendixes in Lotze and Klingner (1997) corresponding to each subseries are given in Table 6. These results and their significance are discussed in following sections of this paper.

Results for eccentric shear tests on two-anchor connections far from free edges (Series 2.5 and 2.6)

In Series 2.5 and 2.6, a two-anchor attachment, with a baseplate that was thick (and therefore presumed rigid) was loaded by eccentric shear. Tests were conducted with eccen-

Table 5—Average loads and displacements at failure for Series 2.4

Test	Edge distance, mm	Failure load, kN	Horizontal displacement, mm	Vertical displacement, mm	Surface dimension of shell-shaped spalling, mm
24M54	140	75.86	0.00	1.19	—
		69.17	1.94	0.41	186
		70.25	2.64	0.52	210
		57.20	2.24	0.25	174
		65.08	3.74	0.00	254
24A54	279	91.28	0.00	1.72	—
		92.69	—*	—*	—
		99.68†	5.10	2.02	—
		90.57‡	6.56	1.91	—

*Measurement failure.

†Only one test.

‡Two tests, one with concrete failure and one with steel failure.

Table 6—Appendixes corresponding to each subseries in Series 2.3 and 2.4

Type of result	Subseries							
	23H64	23H74	23M54	23M74	23M53	23M34	24M54	24A54
Result charts	36	53	64	81	92	108	122	122
Interaction diagram for forces	37	54	65	82	93	109	123	134
Interaction diagram for displacements	38	55	66	83	94	110	124	135
Mathematical description of load-displacement curves	39 to 41	56 to 57	67 to 69	84 to 85	95 to 96	111 to 112	125 to 126	136 to 137
Load-displacement curves	42 to 46	58 to 61	70 to 74	86 to 89	97 to 101	113 to 117	127 to 130	138 to 141
Photos of failure modes	47 to 52	62 to 63	75 to 80	90 to 91	102 to 107	118 to 121	131 to 133	142 to 144

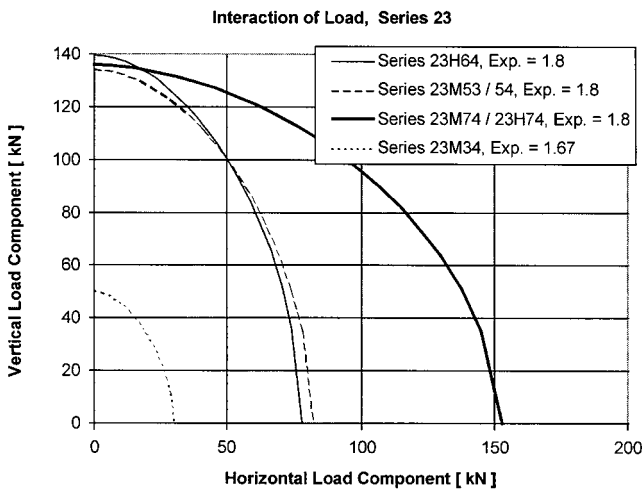


Fig. 10—Interaction curves for actions (Test Series 2.3, Lotze and Klingner 1997).

tricties of 12 in. (305 mm) and 18 in. (457 mm). To reduce friction, a sheet of polytetrafluoroethylene was placed between the concrete and the baseplate. Key test data and the load and displacement measurements are given in Appendix 145 of Lotze and Klingner (1997). Appendix 146 of Lotze and Klingner (1997) contains the results of the measurement of the shell-shaped concrete spalling in the shear direction in front of the anchors. Table 7 is a repetition of the most important results of Series 2.5 and 2.6; the displacement at the center of the baseplate and the rotation were calculated from the vertical displacement measurements. Mean failure loads are given. The calculation of mean deformation data was

abandoned, because the results for each test depend on the hole tolerances and gaps for that test. The appendixes in Lotze and Klingner (1997) corresponding to each subseries are given in Table 8. These results and their significance are discussed in following sections of this paper.

DISCUSSION OF TEST RESULTS

Discussion of results for single anchors loaded at different orientations

Figure 10 is a graph of the mean force interaction diagrams for each subseries of Series 2.3. Plotted on the horizontal and vertical axes, respectively, are the applied tensile and shear loads at failure. In that series, anchor failure was intended to be governed by yield and fracture of anchor steel, so deep embedment depths were used.

Curves for UC1 (Series 23M53 and 23M54) and the sleeve anchor (Series 23H64) are approximately identical. For the tests in 32.4 MPa concrete, this was due to the comparable material characteristics of the anchor shanks and the virtually equal failure displacements under pure tension. In low-strength concrete (20.7 MPa), however, considerably larger failure displacements occurred, especially under tension. Although this obviously has little influence on the interaction of the failure loads associated with the threaded shank, the displacement behavior under oblique tension is affected.

Mean displacement interaction curves for all subseries in Series 2.3 and 2.4 are compared in Fig. 11. Plotted on the horizontal and vertical axes respectively are the applied tensile and shear deformations at failure.

Figure 11 shows large displacements in Series 23M53 under tension, approaching the values achieved in higher strength concrete with increased load angle or increased shear. It also shows good agreement between the values for

Table 7—Loads and displacements at failure for Series 2.5 and 2.6

Test no.	Anchor	Embedment depth, mm	Torque, Nm	Concrete strength, MPa	Failure load, * kN	Horizontal displacement, mm	Vertical displacement, mm	Rotation, degrees	Gap, † mm	Failure mode ‡	
25H642	1	Sleeve M16	178	203/102	34.9	109.55	5.72	1.65	1.50	1.00	SB
	2	Sleeve M16	178	203/102	34.9	110.35	5.31	5.19	2.71	-1.20	SS
	3	Sleeve M16	178	203/102	33.8	111.50	5.50	3.19	1.63	0.60	SS
	Average	110.46									
25H648	1	Sleeve M16	178	203/102	33.8	79.89	5.90	6.56	3.31	1.50	ST
	2	Sleeve M16	178	203/102	33.8	77.93	5.92	5.94	2.95	0.10	ST
	3	Sleeve M16	178	203/102	33.8	77.92	4.18	4.49	2.24	-1.20	ST
	Average	78.58									
25M542	1	UC1 5/8	178	244/122	34.9	106.50	7.42	3.35	2.22	1.20	SS
	2	UC1 5/8	178	244/122	34.9	110.27	7.01	6.24	2.73	-1.40	SS
	3	UC1 5/8	178	244/122	33.8	114.30	9.66	7.77	3.52	1.60	ST
	Average	110.36									
25M548	1	UC1 5/8	178	244/122	34.9	78.95	5.13	8.36	3.99	-1.20	ST
	2	UC1 5/8	178	244/122	33.8	78.39	7.95	8.40	4.30	0.60	ST
	3	UC1 5/8	178	244/122	33.8	87.87	6.73	9.79	5.90	-0.20	ST
	Average	81.74									
25M342	1	UC1 3/8	89	54/27	34.9	36.16	3.88	0.79	0.48	1.00	ST
	2	UC1 3/8	89	54/27	34.9	35.27	—§	0.89	0.50	-2.00	SS
	3	UC1 3/8	89	54/27	34.9	39.45	4.63	1.82	1.10	1.00	ST
	Average	36.96									
25M348	1	UC1 3/8	89	54/27	34.9	26.11	2.66	0.40	0.66	1.50	ST
	2	UC1 3/8	89	54/27	34.9	28.07	3.49	1.05	0.48	1.25	ST
	3	UC1 3/8	89	54/27	34.9	28.16	3.28	1.16	0.87	1.00	ST
	Average	27.44									
26M542	1	UC1 5/8	89	203/122	41.8	74.22	2.97	1.47	0.42	0.80	CT
	2	UC1 5/8	89	203/123	34.2	69.84	2.74	0.99	0.85	-1.20	CT
	3	UC1 5/8	89	203/124	34.2	69.49	3.61	0.66	0.72	-0.40	CT
	Average	71.18									
26M548	1	UC1 5/8	89	203/122	41.8	53.49	2.77	1.36	0.70	-0.30	CT
	2	UC1 5/8	89	203/123	41.8	47.01	2.64	1.44	0.55	0.20	CT
	3	UC1 5/8	89	203/124	34.2	47.71	3.50	0.52	0.50	-1.60	CT
	Average	49.40									

*Values for Series 2.6 with concrete failure normalized by $\sqrt{f_c}/32.4$ MPa.

†Gap before installing nuts: (+) for gaps of shear anchors; (-) for gaps of tension anchors; this anchor different because of wall of hole.

‡ST = steel fracture of tension anchor; SS = steel fracture of shear anchor; SB = steel fracture of both anchors; and CT = concrete breakout at tension anchors.

§Measurement failure.

Table 8—Appendixes corresponding to each subseries in Series 2.5 and 2.6 (Lotze and Klingner 1997)

Type of result	Subseries							
	25H642	25H648	25M542	25M548	25M342	25M348	26M542	26M548
Result charts	145 to 146							
Load-displacement curves and force curves	147 to 149	150 to 152	153 to 155	156 to 158	159 to 161	162 to 164	165 to 167	168 to 170
Photos of failure states	171	172 to 173	173 to 174	174 to 175	176	176	180 to 181	181 to 182
Photos of anchor bolts after tests	177	177	178	178	179	179	182	182

UC1 and the sleeve anchor. Differences are evident, however, due to installation method (through-sleeve versus flush-sleeve). Under pure tension, displacements are identical. At small oblique tension angles, through-sleeve anchor has larger failure displacements than otherwise identical flush-sleeve anchors. The interaction curve for the 3/8 in. (9.5 mm) (Series 23M34, flush-sleeve installation) shows generally smaller displacements than that of the 5/8 in. (16 mm) UC1 but without the distinct maximum displacement at a loading angle of 15 degrees.

In general, anchors installed with flush sleeves and subjected to combined shear and tension generated smaller shell-shaped concrete spalling in the loading direction in front of anchors than did otherwise identical anchors with through sleeves. For this reason, they failed under shear and oblique tension by shear fracture of the anchor shank at a comparatively small shearing deformation. With lower concrete strength, larger displacements were achieved at maximum load under tension. These approach the displacements in higher-strength concrete with increasing shear. Tests with 3/8 in. anchors

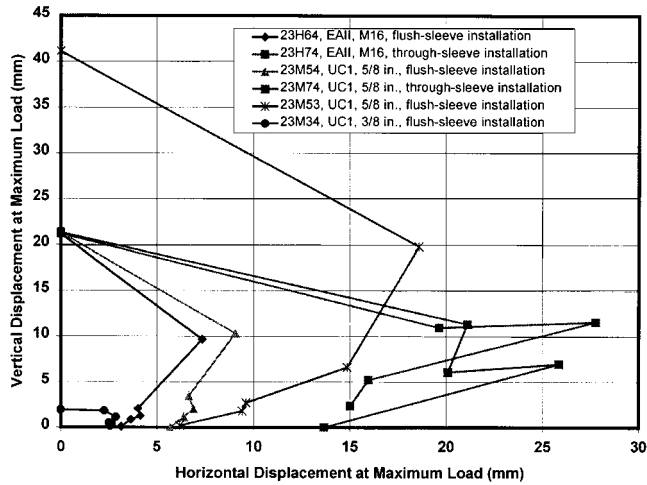


Fig. 11—Interaction curves for displacements (Series 2.3 and 2.4, Lotze 1997).

showed smaller displacements, and no concrete spalling in front of the anchors under shear and oblique tension.

Discussion of results for eccentric shear loading on two-anchor attachments

As shown in Table 7, despite the differences in gaps between anchors and baseplates among specimens, the failure loads of this single test series showed only slight scatter. In contrast, considerable scatter was observed in displacements, without any obvious correlation with the measured gaps.

The gaps, however, did significantly affect the failure mode. In tests with an eccentricity of 18 in. (457 mm), failure always occurred by fracture at the outermost tension anchor. In tests with an eccentricity of 12 in. (305 mm) in Subseries 25H642, 25M542, and 25M342, the shear anchors also fractured. In these three subseries, failure by fracture of the tension anchor occurred only with the largest positive gaps, that is, with maximum gaps of the shear anchors.

Diagrams of the measured displacements, as well as the normal force and bending moment in the baseplate calculated from the strains, are included in Appendixes 147 to 164 (Series 2.5) and 165 to 170 (Series 2.6) of Lotze and Klingner (1997). Post-test photos of the specimen and of the anchors are given in Appendixes 171 to 179 for Series 2.5 and in Appendixes 180 to 182 for Series 2.6 of Lotze and Klingner (1997). (Table 9 shows the Appendixes in Lotze and Klingner [1997] in which results are given for each subseries.)

The graphs of the normal force and bending moment in the baseplate, plotted in the lower diagram in Appendixes 147 to 170 (Lotze and Klingner 1997), were calculated from the results of the strain measurement. Typical results of strain measurement (for Test 25H6423) are plotted in Fig. 12.

The measurement shows that strains are approximately constant over the width of the baseplate, due to its configuration. The large initial strains of different signs in the top versus the bottom of the baseplate indicate the bending moment created by the anchor preload. This can be predicted from the strains using Eq. (9)

$$M = S \cdot \sigma = S \cdot E(\epsilon_{top} - \epsilon_{bottom})/2 \quad (9)$$

where S is the section modulus of baseplate, σ is the bending stress in the baseplate, E is the elastic modulus of steel

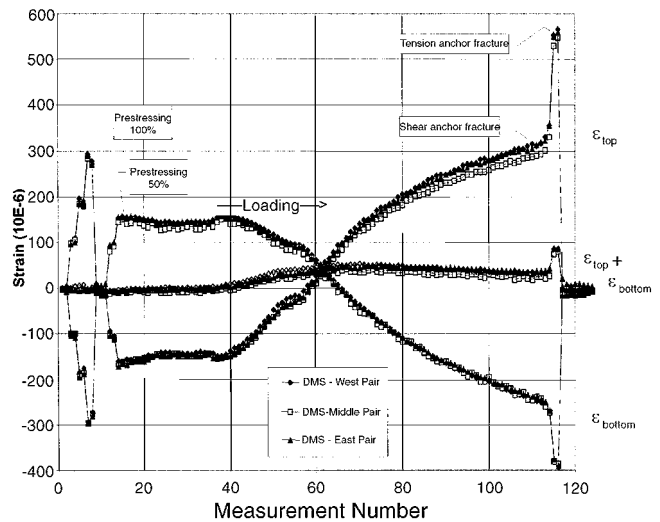


Fig. 12—Strains in Test 25H6423, M16 sleeve, with $h_{ef} = 7$ in. (178 mm) and $e = 12$ in. (305 mm).

(2.1×10^6 MPa), and ϵ_{top} and ϵ_{bottom} are the measured strains at the top and bottom of the baseplate.

The normal force in the baseplate, equal to the shear in the tension anchor, is given by Eq. (10)

$$N = A \cdot E \cdot (\epsilon_{top} + \epsilon_{bottom}) \quad (10)$$

where A is the cross-sectional area of the baseplate.

The relatively small value of $(\epsilon_{top} + \epsilon_{bottom})$ is the summation of the differences between the comparatively large absolute values of the top and the bottom strains. It is therefore sensitive to scatter and inaccuracies in the measured strain value. The normal forces, calculated separately for each of the three pairs of strain gages, are described by sawtoothed curves spaced relatively far apart. Figure 13 shows an example for Test 25H6423. Because all strain-gage pairs provide essentially the same results, the average force (which shows much less scatter than either strain value) is only marginally affected.

Figure 14 shows the diagram of the forces and bending moment in Test 25H6423, as plotted for each test in the Appendixes of Lotze and Klingner (1997). The equation $L = +0.6$ mm in the figure denotes a gap of approximately 0.6 mm in the hole of the baseplate at the shear anchor. As shown in the figure, the normal force in the baseplate (equal to the shear in the tension anchor) increases with the applied load. After the gap at the shear anchor is overcome, this increase slows, and the normal force even decreases at the end. When the shear anchor fractures, the normal force increases abruptly, because the applied shear must then be resisted entirely by the tension anchor.

The hogging bending moment in the baseplate (tensile stresses on top) decreases with increasing external load, changing finally to a reversed moment caused by a combination of the diagonal compression (at the height of the axis of the shear anchor) and the support reaction from the concrete (at the compression edge of the baseplate). The fracture of the shear anchors causes an additional negative moment from the additional normal force of the tension anchor, applied eccentrically to the bottom edge of the baseplate.

Post-failure photos of the tests of Series 2.5 (Appendixes 171 to 176 of Lotze and Klingner [1997]) show generally larg-

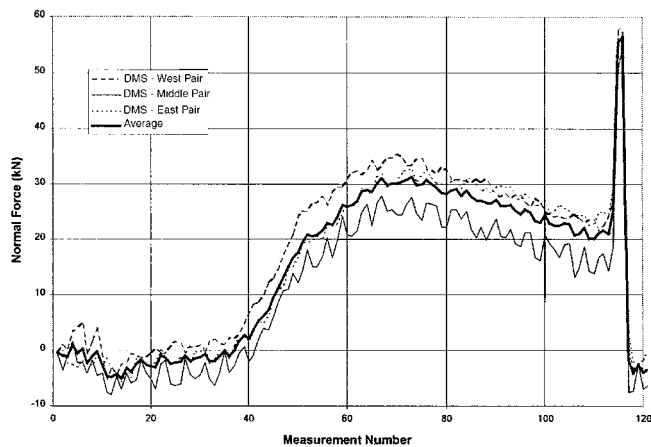


Fig. 13—Normal force in baseplate, calculated separately for each strain-gage pair, Test 25H6423, M16 sleeve anchor, with $h_{ef} = 7$ in. (178 mm) and $e = 12$ in. (305 mm).

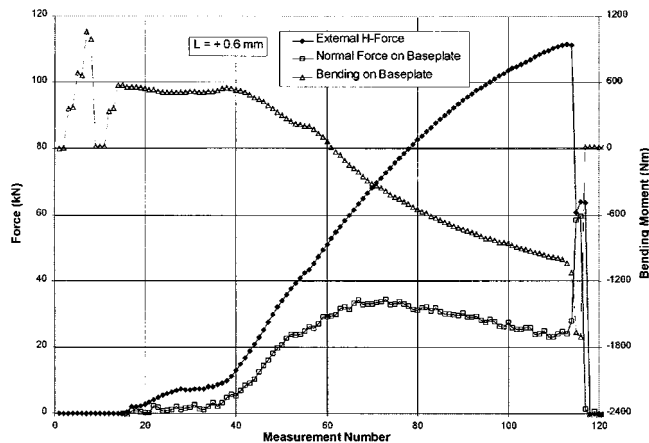


Fig. 14—Force and bending moment of Test 23H6423, M16 sleeve anchor, with $h_{ef} = 7$ in. (178 mm) and $e = 12$ in. (305 mm).

Table 9—Comparison of observed and calculated capacities in Test Series 25M54 (UC1)

Calculation approach	Mean value of observed to predicted capacity		
	$e = 12$ in. (304.8 mm)		$e = 18$ in. (457.2 mm)
	$z_1 = 263$ mm; $z_2 = 9$ mm	$z_1 = 263$ mm; $z_2 = 9$ mm	$z_1 = 284$ mm; $z_2 = 30$ mm
Elastic theory	1.154	1.154	1.085
Plastic theory	0.979	1.050	0.972

er concrete spalling in front of the tension anchors than in front of the shear anchors. This agrees with the results of Series 2.3 overall, in which more spalling was observed at small oblique tension angles. From the photos as well as from measurements of spalling (Appendix 146 of Lotze and Klingner [1997]), the size and depth of the spalling were not influenced by load eccentricity nor anchor type (UC1 versus sleeve). Anchor diameter, however, had a significant effect. The 3/8 in. UC1 showed spalling in only two tests, and these spalls were only 3 to 5 mm deep.

In the photos in Appendixes 177 to 179 of Lotze and Klingner (1997), plastic deformation (necking) is clearly visible in almost all shanks of the broken tension anchors. This points out the ductile fracture behavior of these anchors. On the other hand, the shanks of the shear anchors consistently show small-deformation shear fracture. This confirms the results of Series 2.3, in which under pure shear or at an oblique tension angle greater than 15 to 30 degrees, anchor deformation is small, even with steel failure.

Observed versus predicted capacities for two-anchor attachments with eccentric shear loading

Baseplate moments and axial forces, calculated as explained in the previous section, can be used to calculate the internal distribution of actions among anchors of multiple-anchor attachments. Such distributions can be compared with those calculated by elastic or plastic analysis approaches.

Also useful for this purpose are total predicted capacities. Table 9 through 12 show ratios of observed-to-predicted capacities for the two-anchor attachments tested in Series 2.5 and 2.6. Plastic capacities are calculated using equations presented in Cook and Klingner (1992). One of the variables in those equations is the assumed distance between each row of anchors

Table 10—Comparison of observed and calculated capacities in Test Series 25H65 (sleeve anchor)

Calculation approach	Mean value of observed to predicted capacity		
	$e = 12$ in. (304.8 mm)		$e = 18$ in. (457.2 mm)
	$z_1 = 263$ mm; $z_2 = 9$ mm	$z_1 = 263$ mm; $z_2 = 9$ mm	$z_1 = 284$ mm; $z_2 = 30$ mm
Elastic theory	1.150	1.090	1.030
Plastic theory	0.974	0.978	0.906

and the assumed line of action of the compressive resultant. In this paper, z_1 indicates the assumed lever arm to the farther row of anchors, and z_2 , to the closer row. In some cases, as noted in the tables, the assumed distance was varied.

The results of calculations are plotted in Appendixes 185 through 186, 193 through 194, 201, and 208 of Lotze and Klingner (1997) for each individual test series. The plots of normalized maximum loads over the range of loading eccentricities e permits comparisons among test series independent of the failure load of the anchors used. Besides the calculations of the tests, calculations were carried out with many values of eccentricity e using especially fine increments of e to better show discontinuities in the transition region from failure of shear anchors to fracture of tension anchors.

Using the plastic analysis approach (Cook and Klingner 1992), calculation of the capacity of an attachment loaded in eccentric shear can be categorized into three ranges, according to the eccentricity of the applied shear:

$e < e_1$: Anchors in the compression zone reach their maximum shear capacity. Anchors in the tension zone are loaded in tension and shear;

$e_1 < e < e_2$: Anchors in the compression zone resist that portion of the shear that exceeds the frictional resistance. Anchors in the tension zone are loaded in tension only, and reach their full tension capacity. The connection reaches its maximum flexural capacity; and

$e > e_2$: Shear resistance comes entirely from friction with the concrete. The anchors in the tension zone are loaded in tension only and reach their full tension capacity. The connection reaches its maximum flexural capacity.

In the remainder of this section, the observed results are compared with theoretical predictions. First of all, some common characteristics of results are discussed:

Table 11—Comparison of observed and calculated capacities in Test Series 25M34 (UC1)*

Calculation approach	Mean value of observed to predicted capacity	
	$e = 12$ in. (304.8 mm)	$e = 18$ in. (457.2 mm)
Elastic theory	1.071	1.062
Plastic theory	0.892	0.945

* $z_1 = 263$ mm; $z_2 = 9$ mm.

The capacity of an anchor group loaded in eccentric shear increases as the eccentricity increases from the value corresponding to pure shear ($e = 0$). This is due to friction between the baseplate and the concrete. The additional shear transferred by friction initially exceeds the reduction in shear strength of anchors caused by the additional tension. With further increases in eccentricity, however, the external shear capacity clearly decreases, because the tension anchors always resist less shear. In this region, the failure loads estimated by plastic theory clearly exceed those calculated by elastic theory. For the two-anchor attachments tested in Series 2.5 and 2.6, the difference between the two theoretical curves is greatest at an average eccentricity of 12 in. (300 mm) and decreases to zero at very large eccentricities. For the tested connection, shear redistribution is possible. Tension load redistribution was obviously precluded, however, because only one anchor was present in the tension zone. At large eccentricities, elastic and plastic analysis approaches give essentially the same capacities.

The tests of Series 2.5 and 2.6 were conducted at eccentricities where the differences between the failure loads by elastic theory and by plastic theory were comparatively large, corresponding to significant inelastic redistribution between tension and shear anchors. As shown in Table 9 through 12, observed capacities generally lay between the extremes calculated by elastic and by plastic analysis.

The location of the line of action of the compression resultant between the baseplate and the anchor base has a significant influence on the internal lever arm, and therefore on the failure load of the anchor group. At rotation angles of the baseplate greater than 2.5 degrees, the compression resultant moves quickly to the edge of the baseplate, increasing the internal lever arm of the connection. Baseplate rotations exceeding 2.5 degrees were reached only in Series 25H64 and 25M54 and always with the larger loading eccentricity of 18 in. (457.2 mm).

If failure occurs by fracture of the shear anchors, the horizontal displacement of the group is limited by the failure displacement of the shear anchors, and so is the maximum displacement of the tension anchor.

Results of individual sub-series are given as follows.

Series 25M54 and 25H64 (Table 9 and 10)—The results of Series 25M54 (UC1, flush-sleeve installation, failure by steel fracture) and 25H64 (sleeve anchor, flush-sleeve installation, failure by steel fracture) show consistent behavior despite some differences in the load-displacement behavior of single anchors. Consequently, similar results were observed, and also calculated, for the two-anchor connections with both anchor types. These are therefore discussed together.

Maximum capacity occurred at a loading eccentricity of approximately 12 to 14 in. (305 to 355 mm). At this transition, eccentricity, both the shear and the tension anchors are fully utilized. This was achieved at somewhat larger eccentricities e with the sleeve anchor than with UC1, because the sleeve an-

Table 12—Comparison of observed and predicted capacities in Test Series 26M54 (UC1)*

Calculation approach	Mean value of observed to predicted capacity	
	$e = 12$ in. (304.8 mm)	$e = 18$ in. (457.2 mm)
Elastic theory	0.945	0.954
Plastic theory	0.903	0.941

* $z_1 = 263$ mm; $z_2 = 9$ mm.

chor has a ratio of pure shear to pure tensile capacity of 0.558, compared with 0.607 for UC1. At that transition eccentricity, plastic theory agrees well with the observed capacity, while elastic theory underestimates it by approximately 15%.

For the sleeve anchor at a loading eccentricity of 18 in. (457 mm), plastic theory (including the increased length of the baseplate) accurately predicts capacity. The observed capacity exceeds the calculated value by approximately 2%. Elastic theory underestimates capacity by approximately 9%.

For UC1 (Series 25M54) at a loading eccentricity of 18 in. (457 mm), the expected good agreement between tests and calculations was achieved using the increased baseplate length. The 2 to 3% shortfall of observed to predicted plastic capacity can be explained by the mean observed rotation of 4.73 degrees, compared with the calculated rotation angles of 5 degrees.

Series 25M34 (Table 11)—The results of Series 25M34 are very similar to those of Series 25M54 and 25H64. The maximum ratio of predicted plastic to predicted elastic capacity occurred at a loading eccentricity of about 12 in. (305 mm) and is about 20%. Table 11 shows that plastic theory overestimates the capacity by up to 11%, although the failure was governed by steel fracture and a ductile material was used for the anchors. This is because of the generally smaller failure displacements of the smaller diameter anchors (3/8 in. or M9.5), compared with the larger anchors (5/8 in. or M16) used in Series 25H64 and 25M54.

Series 26M54 (Table 12)—At very small eccentricities of applied load, capacity according to elastic theory is constant, because the predicted capacity is limited by the shear strength of the shear anchors. With plastic theory, however, this does not happen because with even distribution of shear to both anchors (according to elastic theory) plus the superimposed tension on the tension anchor, combined failure of the tension anchor always governs. According to plastic theory, the maximum capacity occurs at an eccentricity of applied load from 3 to 7 in. (75 to 178 mm).

The comparison of observed versus calculated capacities in Table 12 shows that both elastic and plastic analysis methods overpredict capacities. This can be due to the possible overestimation of the strength of the tension anchor based on the very low numbers of tests in Series 24A54. Furthermore, the differences between the elastic and the plastic analysis predictions are smaller than for the other test series. According to plastic theory, the shear anchors are most completely utilized. The real behavior comes relatively close to this assumption because of the low strength of the near-edge shear anchors compared with the tension anchors.

SUMMARY, CONCLUSIONS, AND RECOMMENDATIONS

Summary

This research project, supported by the NRC at the University of Texas at Austin, was intended to assess the seismic behavior of single and multiple-anchor connections in

cracked and uncracked concrete. It addressed single anchors under tensile loading, single anchors under oblique tensile loading, double-anchor connections under tensile loading, single near-edge anchors under shear loading, near-edge double-anchor connections under eccentric shear loading, and multiple-anchor connections under shear at small eccentricities.

This paper summarizes information previously presented in Lotze and Klingner (1997) dealing with Task 2 of that program (behavior of single anchors loaded at different orientations and behavior of two-anchor connections under eccentric shear). The results are used to draw conclusions regarding force and displacement interaction diagrams for single anchors and regarding the applicability of elastic and plastic theory to the design of multiple-anchor connections to concrete.

Conclusions from tests on single anchors loaded at different orientations

Based on the research, the following conclusions may be drawn:

1. The interaction of forces is well-described by an elliptical interaction relationship (Eq. (5)). Based on the present test results, the exponent p is 1.67 to 1.80 for steel failure and 1.6 for concrete fracture;

2. The displacement interaction diagram for steel fracture is bulb-shaped; that is, the shearing displacement at failure under oblique tension is larger than under pure shear. This is due to larger spalling under oblique tension in the direction of the shear, in front of the anchor;

3. In failure by concrete breakout, displacement interaction at maximum load can be approximated by a straight line;

4. Failure by steel fracture and ductile behavior of the steel of anchor shank do not by themselves guarantee ductile behavior of a connection. Brittle fractures of the anchor shank can occur depending on concrete strength, anchor size, installation method, and loading direction, especially when shear dominates. Low steel strength, small anchor diameters, flush-sleeve installation, and high-strength concrete lead to small deformation capacity; and

5. Ductile fractures will be achieved, in principle, if the maximum possible steel strength of the anchor is reached. Therefore, connections with large edge distance, higher-strength yet ductile steels, and through-sleeve installation (sleeve extending to the top surface of baseplate) are recommended.

Conclusions from eccentric shear tests on two-anchor connections

Based on the research, the following conclusions may be drawn:

1. For large eccentricity in shear (capacity governed by fracture of the tension anchor), plastic theory accurately predicts connection behavior and capacity;

2. At lower eccentricities of applied shear, the bulb-shaped interaction curve for displacements causes a failure transition from the tension anchor to the shear anchor. At this point, both shear anchors and tension anchors are fully utilized,

and the assumptions of plastic theory agree with the actual behavior of the connection; and

3. At still lower eccentricities of applied shear, the transverse displacement of the tension anchor cannot exceed the transverse displacement of the shear anchor. For that reason, the tension anchors of a multiple-anchor connection cannot reach the fracture states in the belly of the displacement interaction curve. Contrary to the assumptions of plastic theory, this causes the strength of the tension anchor to be under-utilized at small loading eccentricities. Depending on how pronounced the belly of the interaction curve is, the calculated capacity of the group can be considerably over-estimated by plastic theory, or even by elastic theory. Lotze and Klingner (1997) propose that this problem be corrected by assuming an even distribution of shear to all anchors.

ACKNOWLEDGMENTS AND DISCLAIMER

This paper presents partial results of a research program supported by the U.S. Nuclear Regulatory Commission (NUREG/CR-5434, "Anchor Bolt Behavior and Strength during Earthquakes"). The technical contact is Herman L. Graves, III, whose support is gratefully acknowledged. The conclusions in this paper are those of the authors only and are not NRC policy or recommendations.

REFERENCES

- Bode, H., and Roik, K., 1987, "Headed Studs Embedded in Concrete and Loaded in Tension," *Anchorage to Concrete*, SP-103, G. B. Hasselwander, ed., American Concrete Institute, Farmington Hills, Mich., pp. 61-88.
- CEB, 1991, "Fastenings to Reinforced Concrete and Masonry Structures: State-of-the-Art Report, Part 1," Euro-International Concrete Committee.
- Cook, R. A., and Klingner, R. E., 1992, "Ductile Multiple-Anchor Steel-to-Concrete Connections," *Journal of Structural Engineering*, V. 118, No. 6, June, pp. 1645-1665.
- Dieterle, H.; Bozenhardt, A.; Hirth, W.; and Opitz, V., 1989, "Tragverhalten von nicht generell zugzonentauglichen Dübeln, Teil 4: Verhalten im unbewegten Parallelriß unter Schrägzugbelastung," *Bericht Nr. 1/45-89/19*, Institut für Werkstoffe im Bauwesen, Universität Stuttgart.
- Eligehausen, R.; Fuchs, W.; Lotze, D.; and Reuter, M., 1989, "Befestigungen in der Betonzugzone," *Beton und Stahlbetonbau*, No. 1, pp. 27-32, No. 2, pp. 71-74.
- Fuchs, W., 1990, "Tragverhalten von Befestigungen unter Querlast in ungerissenem Beton," Dissertation, Universität Stuttgart, 1990.
- Fuchs, W.; Eligehausen, R.; and Breen, J. E., 1995, "Concrete Capacity Design (CCD) Approach for Fastening to Concrete," *ACI Structural Journal*, V. 92, No. 1, Jan.-Feb., pp. 73-94.
- International Conference of Building Officials (IBC), 2000, "International Building Code," Whittier, Calif.
- Johnson, M., and Lew, H., 1990, "Experimental Study of Post-Installed Anchors under Combined Shear and Tension Loading," *Anchorage to Concrete*, SP-103, G. B. Hasselwander, ed., American Concrete Institute, Farmington Hills, Mich.
- Klingner, R. E.; Hollowell, J. M.; Lotze, D.; Park, H.-G.; Rodriguez, M.; and Zhang, Y.-G., 1998, *Anchor Bolt Behavior and Strength during Earthquakes*, Report prepared for the U.S. Nuclear Regulatory Commission (NUREG/CR-5434).
- Lotze, D., and Klingner, R. E., 1997, "Behavior of Multiple-Anchor Connections to Concrete From the Perspective of Plastic Theory," *PMFSEL Report No. 96-4*, University of Texas at Austin.
- McMackin, P. J.; Slutter, R. G.; and Fishere, J. W., 1973, "Headed Steel Anchor under Combined Loading," *Engineering Journal*, AISC, V. 10, No. 2.
- Prestressed Concrete Institute (PCI), 1985, *PCI Design Handbook—Precast and Prestressed Concrete*, 3rd Edition, Chicago, Ill.
- Rehm, G.; Eligehausen, R.; and Mallée, R., 1992, "Befestigungstechnik," *Betonkalender*, pp. 569-663.
- Shaikh, A., and Whayong, Y., 1985, "In-Place Strength of Welded Headed Studs," *Journal of the Prestressed Concrete Institute*, pp. 56-81.